materials

MDPI

Article

Crystallization Behavior of $Al_{70}Fe_{12.5}V_{12.5}Nb_5$ Amorphous Alloy Formed by Mechanical Alloying

Xuan Liu [1,2,3], Xingfu Wang [1], Yongli Si [1,2], Xiaokang Zhong [1,2] and Fusheng Han [1,*]

[1] Key Laboratory of Materials Physics, Institute of Solid State Physics, Chinese Academy of Science, Hefei 230031, China; liuxuan@ahjzu.edu.cn (X.L.); wangxingfu@issp.ac.cn (X.W.); siyongli@mail.ustc.edu.cn (Y.S.); xkzhong@mail.ustc.edu.cn (X.Z.)
[2] University of Science and Technology of China, Hefei 230026, China
[3] College of Civil Engineering, Anhui Jianzhu University, Hefei 230061, China
* Correspondence: fshan@issp.ac.cn

Received: 19 December 2018; Accepted: 22 January 2019; Published: 26 January 2019

Abstract: In this study, the formation and crystallization of the $Al_{70}Fe_{12.5}V_{12.5}Nb_5$ amorphous alloys has been investigated. The addition of Nb enhances the supercooled liquid region and glass forming ability of the Al-Fe-V amorphous alloys. The $Al_{70}Fe_{12.5}V_{12.5}Nb_5$ amorphous alloy exhibits two distinct crystallization steps and a large supercooled liquid region at more than 100 K. Kissinger and Ozawa analyses showed that the two activation energies for crystallization (E_x) were estimated to be 366.3 ± 23.9 and 380.5 ± 23.9 kJ/mol. Large supercooled liquid regions are expected to gain an application field of Al-based amorphous alloys.

Keywords: aluminum-based amorphous alloys; mechanical alloying; supercooled liquid region; Nb addition

1. Introduction

Currently, the application of amorphous powder in bulk metallic glasses, composite, coating, and 3D printing has widened the application scope of amorphous alloys [1–4]. In particular, Aluminum-based amorphous alloys have attracted increasing attention due to their exceptional physical properties, low glass forming ability (GFA), and poor thermal stability [5–7]. However, Al-based amorphous alloys with low GFA are challenging to be synthesized via the traditional rapid quenching (RQ). The size factor restricts the practical application of Aluminum-based amorphous alloys. Indeed, up to now, the maximum diameter of an Al-based amorphous alloys sample is 2.5 mm by RQ [8]. Mechanical alloying (MA) is an effective process to produce amorphous alloy powders without a high cooling rate [9,10]. Therefore, it is noteworthy to prepare Al-based amorphous powders via MA to widen their application [11–15]. To use amorphous powder, a large supercooled liquid region (ΔT_x) is necessary, and enhancement of the GFA and thermal stability is required.

The addition of Nb can improve the GFA, thermal stability, and the corrosion resistance of Zr-based Zr-Ni-Al-Nb bulk metallic glasses with high compressive yield strength [16]. A similar phenomenon has been observed in some Al-based amorphous alloys [17,18]. It has been reported that, in the case of the Nb-Al system, the sequence of phase formation varies widely depending upon Al content: for example, $Al_{80}Fe_{10}Nb_{10}$ created via an MA process lasted 100 h is a powder mixture [19,20]. However, according to the efficient cluster packing (ECP) model, Nb has the same atomic radius as Al, so they can be mixed with an arbitrary ratio to occupy the Ω position of the solvent atoms without changing the cluster packing structure in the amorphous alloys [21]. Thus, it is interesting to investigate the GFA and thermal stability of in Al-based amorphous alloys in which Nb has replaced Al. $Al_{75}V_{12.5}Fe_{12.5}$ amorphous alloys with high GFA and thermal stability were prepared via MA and

based on the ECP model [22]. In general, a negative heating of the mixing enthalpy (ΔH_{mix}) among elements in the amorphous alloy is beneficial for enhancing the GFA [23]. Nb contribution to the enthalpy leads to a negative ΔH_{mix} with Al (−18 kJ/mol), Fe (−16 kJ/mol), and V (−1 kJ/mol) [24]. Therefore, the GFA and thermal stability expect to be enhanced with the Nb addition in the Al-Fe-V alloys. In this work, we synthesized alloys with 5% of Al replaced by Nb. The GFA and thermal stability were investigated according to the values obtained from differential scanning calorimetry (DSC). The aim of this study is to obtain Al-based amorphous powder with high ΔT_x and thermal stability for industrial applications.

2. Experimental Details

The $Al_{70}Fe_{12.5}V_{12.5}Nb_5$ (at %) amorphous alloy powders were prepared via MA of a mixture of elemental Al (99.9%), Fe (99.8%), V (99.9%), and Nb (99.7%) powders. Stearic acid powder (2 wt. %) was used as the process control agent. The MA was conducted in a high-energy planetary ball mill (QM-3SP4, Instrument Factory of Nanjing University, Nanjing, China) using a stainless steel vial and a steel ball bearing (GGr15 with diameters of 20 mm, 10 mm, and 5 mm are mixed) with the rotation speed of 350 rpm and ball-to-powder weight ratio of 20:1 in a highly pure Ar atmosphere. The vial is introduced into the vacuum glove box every 10 h to obtain the powder samples for analysis. The powder samples were characterized via X-ray diffraction (XRD, X' Pert Pro MPD, Philips) using Cu Ka radiation in the 2θ range of 20° to 90°. The X'Pert HighScore Plus software (Version: 3.0) is used to analyze the XRD curves of the mixed powder after ball milling. The microstructures of the amorphous powders were examined using transmission electron microscopy (TEM, JEOL 2010, JEOL) and selected area electron diffraction (SAED) operating at 200 kV. The thermal properties, such as T_g (the glass transition temperature), T_x (the onset crystallization temperature), T_{p1} (the first crystallization peak temperature), T_{p2} (the secondary crystallization peak temperature), T_m (the melting temperature), T_l (the liquidus temperature), were measured via the DSC (NETZSCH DSC 404F3) at heating rates of 10, 20, 30, 40 K/min from 303 K to 1473 K in an Ar atmosphere.

3. Results and Discussion

XRD results of $Al_{70}Fe_{12.5}V_{12.5}Nb_5$ alloy powders milled for different periods (10 h, 20 h, 30 h, 40 h, 50 h and 60 h) are shown in Figure 1. It can be seen from Figure 1 that the crystalline phase is formed by ball milling 10 h, X'Pert HighScore Plus software results suggest that the crystalline phase is $AlNb_2$. With the increase of milling time, no new diffraction peaks have been found in the XRD curve, indicating that no new crystalline phase is formed except for $AlNb_2$. From the DSC curve of 10 h to 30 h, the intensity of the diffraction peak corresponding to the initial addition of powder elements is reduced with the strongest diffraction peak position moving towards higher 2θ angles of 0.2°. According to the Scherrer formula, this means that the lattice of Al has infiltrated other atoms with a smaller atomic radius and formed a solid solution. The atomic radius of Fe (0.124 nm) and V (0.132 nm) is shorter than the radius of Al (0.143 nm); therefore, the product is the Al-Fe-V solid solution formed by Fe and V dissolved in Al. When milling to 40 h, the diffraction peak still exists and has broadened, indicating that the amorphous phase is formed and there are crystalline phases and solid solutions at this time. After milling 50 h, the diffraction peaks of all crystals disappear, while different diffuse peaks can be identified at a 2θ angle of 37°. Until the 60 h milling treatment, only the typical broad halo peak showing the amorphous structure exists, indicating that the powders are amorphous.

To verify the amorphous structure, the TEM and selected area electron diffraction (SEAD) images of $Al_{70}Fe_{12.5}V_{12.5}Nb_5$ alloys powder milled for 60 h are shown in Figure 2. There is no visible crystals in the TEM image, and the broad diffuse halo and the absence of rings or diffraction spots in the SEAD pattern further confirms the amorphous structure.

The GFA and thermal stability of the amorphous alloy are related to atomic radii mismatch and thermodynamics of the alloy systems: it can be displayed by the milling time of MA amorphous

powders. Compared with the $Al_{75}V_{12.5}Fe_{12.5-x}Cu_x$ amorphous alloys reported in the literature [22], the $Al_{70}Fe_{12.5}V_{12.5}Nb_5$ amorphous alloy milling time is reduced.

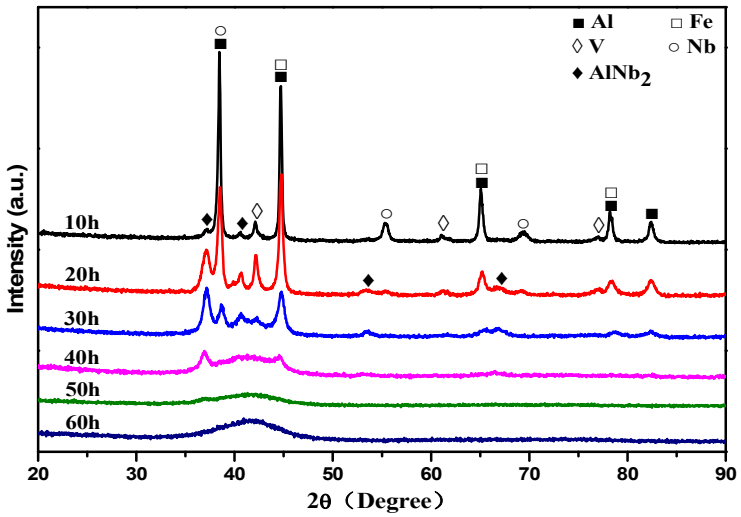

Figure 1. X-ray diffraction patterns (XRD) patterns of $Al_{70}Fe_{12.5}V_{12.5}Nb_5$ powders milled for 10, 20, 30, 40, 50 and 60 h.

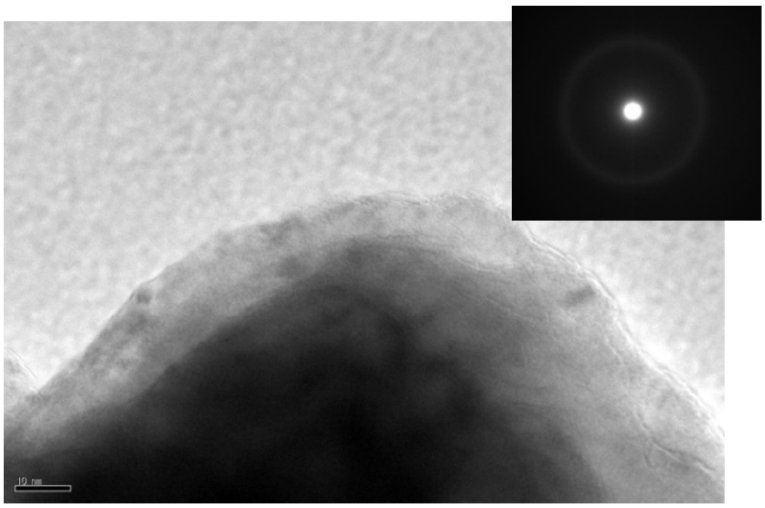

Figure 2. Transmission electron microscope (TEM) image and selected area electron diffraction (SAED) pattern of $Al_{70}Fe_{12.5}V_{12.5}Nb_5$ alloys powder milled for 60 h.

The parameter *Delta* is adopted to describe the effect of atomic radii mismatch of multi-component alloys as follows [25]:

$$Delta = \sqrt{\sum_{i=1}^{n} c_i(1 - r_i/\overline{r})^2}. \quad (1)$$

Here, the n is the number of components in the amorphous alloy system, c_i is the atomic percentage of the i component, and r_i is the atomic radius, $\overline{r}$ ($\overline{r} = \sum_{i=1}^{n} c_i r_i$) is the average atomic radius.

By calculating the *Delta*, the $Al_{70}Fe_{12.5}V_{12.5}Nb_5$ and $Al_{75}V_{12.5}Fe_{12.5-x}Cu_x$ amorphous alloys have the same value. We can then infer that the influence of atomic radii mismatch of the two systems can be neglected.

Another parameter, the equation of the Gibbs free energy (ΔG_{mix}), is used to characterize the thermodynamics of alloy systems.

$$\Delta G_{mix} = \Delta H_{mix} - T\Delta S_{mix}. \quad (2)$$

According to Equation (2), a low mixing enthalpy (ΔH_{mix}) or a high entropy of mixing (ΔS_{mix}) can decrease the ΔG_{mix}, thus lowering the crystallization driving force, which consequently renders the formation of the amorphous phase easier. ΔH_{mix} and ΔS_{mix} can be calculated by Equations (3) and (4), respectively.

$$\Delta H_{mix} = \sum_{i=1, i\neq j}^{n} \Omega_{ij} c_i c_j, \tag{3}$$

$$\Delta S_{mix} = -R \sum_{i=1, i\neq j}^{n} c_i Ln c_i, \tag{4}$$

where $\Omega_{ij} = 4\Delta H_{ij}$, the ΔH_{ij} is the mixing enthalpy of the i and j elements, and R is the gas constant. It can be concluded that the ΔH_{mix} increases in the order of the $Al_{70}Fe_{12.5}V_{12.5}Nb_5$ (−11.970 kJ/mol), $Al_{75}V_{12.5}Fe_{12.5}$ (−10.125 kJ/mol), $Al_{75}V_{12.5}Fe_{6.25}Cu_{6.25}$ (−8.250 kJ/mol), $Al_{75}V_{12.5}Cu_{12.5}$ (−6.375 kJ/mol) amorphous alloys. The ΔS_{mix} decreases in the order of the $Al_{70}Fe_{12.5}V_{12.5}Nb_5$ (0.919R), $Al_{75}V_{12.5}Fe_{12.5}$ (0.736R), $Al_{75}V_{12.5}Cu_{12.5}$ (0.736R), $Al_{75}V_{12.5}Fe_{6.25}Cu_{6.25}$ (0.649R) amorphous alloys. In these amorphous alloys, $Al_{70}Fe_{12.5}V_{12.5}Nb_5$ has the lowest ΔH_{mix} and the highest ΔS_{mix}, so the ΔG_{mix} is the lowest according to Equation (2). This may be the reason why the $Al_{70}Fe_{12.5}V_{12.5}Nb_5$ amorphous alloy milling time is shortest among these amorphous alloys. Thus, we conclude that the GFA and thermal stability of $Al_{70}Fe_{12.5}V_{12.5}Nb_5$ amorphous alloy are higher than $Al_{75}V_{12.5}Fe_{12.5-x}Cu_x$ amorphous alloys.

Figure 3a shows the DSC curves of the $Al_{70}Fe_{12.5}V_{12.5}Nb_5$ amorphous alloy at the heating rates of 10, 20, 30, and 40 K/min. Two exothermic crystallization events can be observed and are associated with the transformations from an amorphous state to the equilibrium phases. The temperature of T_g that indicates glass transition at the different heating rate (see Figure 3b). The thermal properties of T_g, T_x, T_{p1}, T_{p2}, T_m, T_l are marked with arrows in Figure 3a and listed in Table 1, which also contains the empirical criteria of GFA [23,26], ΔT_x ($\Delta T_x = T_x - T_g$), the reduced glass transition temperature T_{rg}($T_{rg} = T_g/T_l$), the γ val ($\gamma = T_x/(T_g + T_l)$). It is clear that, with the increase of heating rate, T_g, T_x, T_{p1}, T_{p2}, turn to a higher temperature, while the ΔT_x fluctuates between 106.5 and 117.5 K. This shows that the thermal properties of $Al_{70}Fe_{12.5}V_{12.5}Nb_5$ at different heating rates are influenced by kinetic factors. The values of T_x and ΔT_x of $Al_{70}Fe_{12.5}V_{12.5}Nb_5$ amorphous alloy are 854.1 K and 118.6 K at the heating rates of 20 K/min, respectively, whereas the T_m is almost unchanged. It should be noted that the change of ΔT_x for $Al_{70}Fe_{12.5}V_{12.5}Nb_5$ is more than 100 K, which is higher than $Al_{75}V_{12.5}Fe_{12.5-x}Cu_x$ amorphous alloys and other Al-based amorphous alloys [27]. The higher ΔT_x,T_{rg}, γ indicates that the $Al_{70}Fe_{12.5}V_{12.5}Nb_5$ amorphous alloy has a higher glass forming ability. Therefore, it is a promising candidate for thermoplastic forming BMGs and composite materials via the consolidation of amorphous powders.

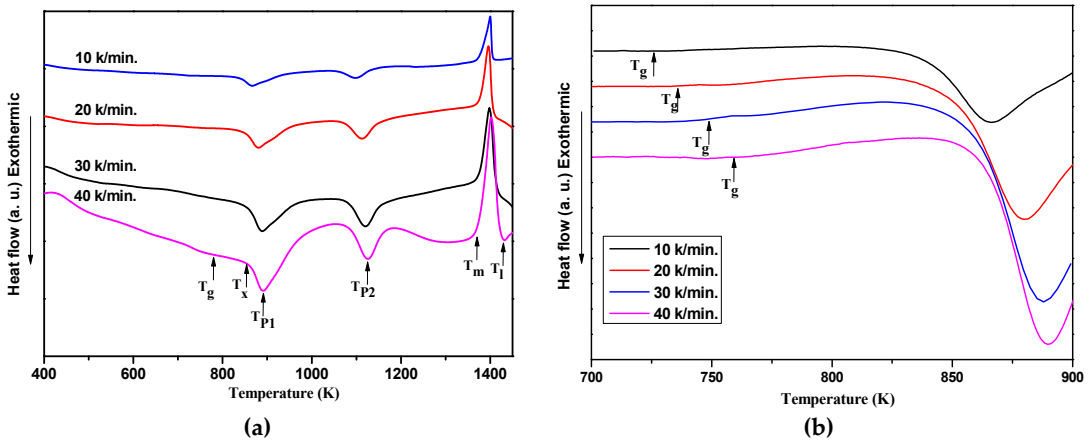

Figure 3. (**a**) Differential scanning calorimetry (DSC) curves of the $Al_{70}Fe_{12.5}V_{12.5}Nb_5$ amorphous alloy at the heating rates of 10, 20, 30, and 40 K/min. (**b**) Enlarged area of the DSC curves shown in (**a**) of the T_g.

Table 1. The thermal properties and ΔT_x, T_{rg}, γ of $Al_{70}Fe_{12.5}V_{12.5}Nb_5$ measured at 10, 20, 30, and 40 K/min heating rates.

β(K/min)	T_g(K)	T_x (K)	T_{p1} (K)	T_{p2} (K)	T_m(K)	T_l (K)	ΔT_x(K)	T_{rg}	γ
10	726.7	844.2	866.2	1097.7	1375.2	1408.7	117.5	0.516	0.395
20	736.9	854.1	881.0	1112.4	1377.9	1407.9	117.2	0.522	0.398
30	749.8	862.5	888.8	1120.1	1377.5	1416.9	112.7	0.529	0.398
40	759.0	865.5	890.9	1125.7	1376.5	1427.3	106.5	0.532	0.396

The activation energies of E_x, E_{p1}, E_{p2} corresponding to T_x, T_{p1}, T_{p2}, respectively, can be estimated via the equations of Kissinger (Equation (5)) and Ozawa (Equation (6)) [28,29]:

$$\mathrm{Ln}\left(\beta/T^2\right) = -(E/RT) + \mathrm{Const} \quad (5)$$

$$\mathrm{Ln}\left(\beta\right) = -(E/RT) + \mathrm{Const} \quad (6)$$

Here, the β is the heating rates, T represents the specific temperature (T_x, T_{p1}, T_{p2}), E is the corresponding activation energy (E_x, E_{p1}, E_{p2}), and R is the gas constant.

Figure 4 reports the Kissinger and Ozawa plots by linear fitting of ln (β/T^2) versus 1/T or ln (β) versus 1/T. The estimated activation energies (E_x, E_{p1}, E_{p2}) corresponding to T_x, T_{p1}, T_{p2} were evaluated by the Kissinger and Ozawa methods, and listed in Table 2. The fitted curves are close to the straight lines; the Adjusted R-square is higher than 96, and the results of the two equations have the same tendency, which proves the reliability of the data. It is clear that the effective activation energies evaluated by the Kissinger equation are smaller than Ozawa equation. The E_x values resulting by the application of the Kissinger and Ozawa methods can be calculated: 366.3 ± 23.9 and 380.5 ± 23.9 kJ/mol, respectively.

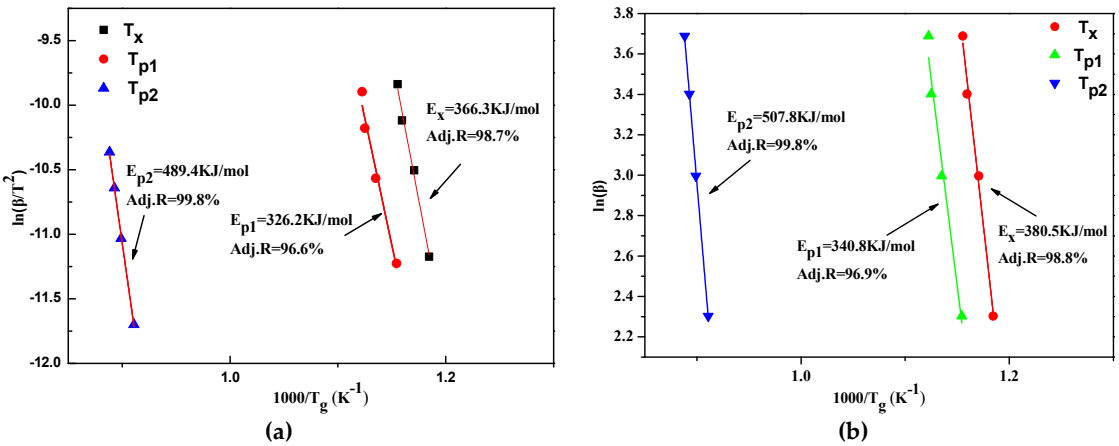

Figure 4. The Kissinger and Ozawa plots of T_x, T_{p1}, $T_{p2}$of the $Al_{70}Fe_{12.5}V_{12.5}Nb_5$ amorphous alloy. (**a**) Kissinger plot, (**b**) Ozawa plot.

Table 2. Energies of E_x, E_{p1}, E_{p2} estimated with the Kissinger and Ozawa methods.

Equations	E_x (KJ/mol)	E_{p1} (KJ/mol)	E_{p2} (KJ/mol)
Kissinger	366.3 ± 23.9	326.2 ± 35.0	489.4 ± 12.2
Ozawa	380.5 ± 23.9	340.8 ± 35.0	507.8 ± 12.2

The DSC curves in Figure 3 have two obvious endothermic peaks, which means that there are two crystallization processes. To further understand the crystallization of the new crystalline phases during the exothermic processes, five heat treatments of the $Al_{70}Fe_{12.5}V_{12.5}Nb_5$ amorphous alloy powders were studied. Figure 5 shows the XRD pattern of the $Al_{70}Fe_{12.5}V_{12.5}Nb_5$ amorphous alloy powders

after five different heat treatments. Different heat treatment temperatures have been selected: 773 K (below T_x and above T_g), 973 K (between T_{P1} and T_{P2}), and 1173 K (above T_{P2}).

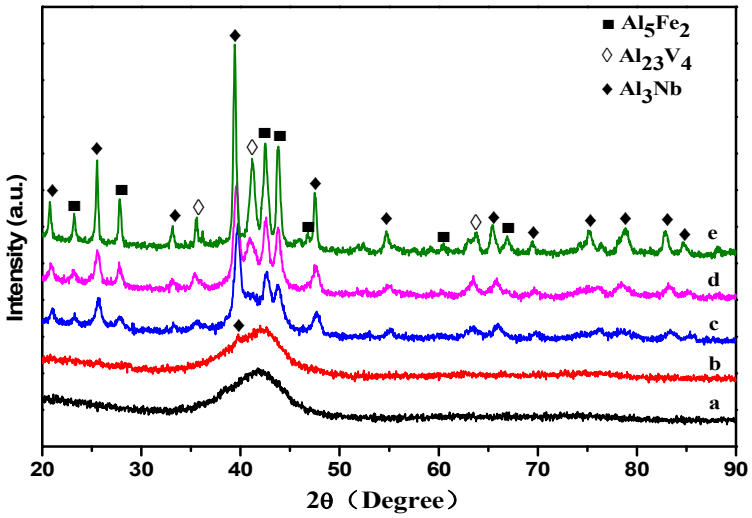

Figure 5. XRD patterns of the $Al_{70}Fe_{12.5}V_{12.5}Nb_5$ amorphous alloy powders after heat treatment: (a) fast cooling after heating to 773 K; (b) annealing at 773 K for 100 min; (c) fast cooling after heating to 973 K; (d) annealing at 973 K for 100 min; (e) fast cooling after heating to 1173 K.

The crystal phase is not observed when the sample has been heated to 773 K before rapid cooling (heat treatment *a* in Figure 5). When amorphous alloy samples are annealed at 773 K for 100 min (heat treatment *b*), a few Al_3Nb phases of the amorphous sample can be observed. It is shown that the short-range atom structure retained in the amorphous alloy has been partly changed after low-temperature annealing, while a certain degree of relaxation has occurred. Although the crystallization temperature has not been reached, the atom diffusion ability of the amorphous alloy has increased after annealing for 100 min with the Nb addition. Al_5Fe_2 and Al_3Nb phases have been mainly observed after initial crystallization and rapid cooling immediately after heating to 973 K (heat treatment *c*). The $Al_{23}V_4$ phase is also found at 973 K annealing for 100 min (heat treatment *d*) and heating to 1173 K (heat treatment *e*). New crystalline phases precipitate when the amorphous sample is annealed, which may be due to the relaxation of the amorphous structure. To reduce the internal free energy of the amorphous alloy, a certain crystallization phase has precipitated in the amorphous alloy.

4. Conclusions

Amorphous alloy $Al_{70}Fe_{12.5}V_{12.5}Nb_5$ (at %) powders were successfully prepared via MA. The replacement of Al with Nb in the $Al_{75}V_{12.5}Fe_{12.5}$ amorphous alloy effectively enhances its glass forming ability and thermal stability. The $Al_{70}Fe_{12.5}V_{12.5}Nb_5$ amorphous alloy exhibits a larger supercooled liquid region than 100 K, higher GFA with the T_{rg} of 0.522, and γ of 0.398 (20 K/min). The crystallization of the $Al_{70}Fe_{12.5}V_{12.5}Nb_5$ amorphous alloy takes place in two distinct steps, as observed via DSC analyses. Our study provides deeper insights into the development of Al-base amorphous alloys to be used in powder metallurgy industry.

Author Contributions: Conceptualization, X.L. and F.H.; methodology, X.L.; software, X.W.; validation, Y.S. and X.Z.; formal analysis, X.L.; investigation, X.L.; resources, Y.S.; data curation, Y.S.; writing—original draft preparation, X.L.; writing—review and editing, F.H.; visualization, F.H.; supervision, F.H.; project administration, F.H.; funding acquisition, X.L.

Funding: This research was funded by the National Natural Science Foundation of China (51371167). Anhui Provincial Universities Natural Science Research Project (KJ2016JD03).

Conflicts of Interest: The authors declare no conflict of interest.

References

1. Maurya, R.S.; Sahu, A.; Laha, T. Effect of sintering temperature on phase transformation during consolidation ofmechanically alloyed $Al_{86}Ni_6Y_6Co_2$ amorphous powders by spark plasma sintering. *J. Non-Cryst. Solids* **2016**, *453*, 1–7. [CrossRef]
2. Zhang, L.; Yang, L.; Leng, J.; Wang, T.; Wang, Y. Alloying Behavior and Properties of Al-Based Composites Reinforced with $Al_{85}Fe_{15}$ Metallic Glass Particles Fabricated by Mechanical Alloying and Hot Pressing Consolidation. *JOM* **2017**, *69*, 748–755. [CrossRef]
3. Gao, M.; Lu, W.; Yang, B.; Zhang, S.; Wang, J. High corrosion and wear resistance of Al-based amorphous metallic coating synthesized by HVAF spraying. *J. Alloys Compd.* **2018**, *735*, 1363–1373. [CrossRef]
4. Li, N.; Zhang, J.; Xing, W.; Ouyang, D.; Liu, L. 3D printing of Fe-based bulk metallic glass composites with combined high strength and fracture toughness. *Mater. Des.* **2018**, *143*, 285–296. [CrossRef]
5. Liao, J.P.; Yang, B.J.; Zhang, Y.; Lu, W.Y.; Gu, X.J.; Wang, J.Q. Evaluation of glass formation and critical casting diameter in Al-based metallic glasses. *Mater. Des.* **2015**, *88*, 222–226. [CrossRef]
6. Yin, J.; Cai, H.; Cheng, X.; Zhang, X. Al-based bulk metallic glass with large plasticity and ultrahigh strength. *J. Alloys Compd.* **2015**, *648*, 276–279. [CrossRef]
7. Wu, N.C.; Zuo, L.; Wang, J.Q.; Ma, E. Designing aluminum-rich bulk metallic glasses via electronic-structure-guided microalloying. *Acta Mater.* **2016**, *108*, 143–151. [CrossRef]
8. Yang, B.J.; Lu, W.Y.; Zhang, J.L.; Wang, J.Q.; Ma, E. Melt fluxing to elevate the forming ability of Al-based bulk metallic glasses. *Sci. Rep.* **2017**, *7*, 1–16. [CrossRef] [PubMed]
9. Koch, C.C. Materials Synthesis by Mechanical Alloying. *Annu. Rev. Mater. Res.* **1989**, *19*, 121–143. [CrossRef]
10. Suryanarayana, C. Mechanical Alloying and Milling. *Prog. Mater. Sci.* **2001**, *46*, 1–184. [CrossRef]
11. Mula, S.; Mondal, K.; Ghosh, S.; Pabi, S.K. Structure and mechanical properties of Al–Ni–Ti amorphous powder consolidated by pressure-less, pressure-assisted and spark plasma sintering. *Mater. Sci. Eng. A* **2010**, *527*, 3757–3763. [CrossRef]
12. Tan, Z.; Wang, L.; Xue, Y.; Cheng, X.; Zhang, L. structural modification of $Al_{65}Cu_{16.5}Ti_{18.5}$ amorphous powder through annealing and post milling, improving thermal stability. *J. Mater. Sci. Technol.* **2016**, *32*, 1326–1331. [CrossRef]
13. Maurya, R.S.; Sahu, A.; Laha, T. Quantitative phase analysis in $Al_{86}Ni_8Y_6$ bulk glassy alloy synthesized by consolidating mechanically alloyed amorphous powder via spark plasma sintering. *Mater. Des.* **2016**, *93*, 96–103. [CrossRef]
14. Nguyen, V.H.; Nguyen, O.T.; Dudina, D.V.; Le, V.V.; Kim, J.S. Crystallization Kinetics of Al-Fe and Al-Fe-Y Amorphous Alloys Produced by Mechanical Milling. *J. Nanomater.* **2016**, *2*, 1–9. [CrossRef]
15. Tan, Z.; Xue, Y.F.; Cheng, X.W.; Zhang, L.; Chen, W.W.; Wang, L.; Zhang, H.F.; Fu, H.M. Effect of element fitting on composition optimization of Al-Cu-Ti amorphous alloy by mechanical alloying. *Trans. Nonferrous Met. Soc. China* **2015**, *25*, 3348–3353. [CrossRef]
16. Li, Y.H.; Zhang, W.; Dong, C.; Qiang, J.B.; Xie, G.Q.; Fujita, K.; Inoue, A. Enhancement of glass-forming ability and corrosion resistance of Zr-based Zr-Ni-Al bulk metallic glasses with minor addition of Nb. *J. Appl. Phys.* **2011**, *110*, 023513. [CrossRef]
17. Wu, Y.; Wang, X.F.; Han, F.S. Preparation of $Al_{72}Ni_8Ti_8Zr_6Nb_3Y_3$ amorphous powders and bulk materials. *Int. J. Min. Met. Mater.* **2016**, *23*, 1187–1195. [CrossRef]
18. Mostaan, H.; Karimzadeh, F.; Abbasi, M.H. Thermodynamic analysis of nanocrystalline and amorphous phase formation in Nb–Al system during mechanical alloying. *Powder Metall.* **2012**, *55*, 142–147. [CrossRef]
19. Tavoosi, M.; Karimzadeh, F.; Enayati, M.H. Formation and characterization of amorphous–nanocrystalline $Al_{80}Fe_{10}M_{10}$ [M = Fe, Nb, Ti, Ni, (Ni0.5Ti0.5)] alloys. *J. Alloys Compd.* **2013**, *551*, 584–590. [CrossRef]
20. Peng, Z.; Suryanarayana, C.; Froes, F.S. Mechanical alloying of Nb-Al powders. *Metall. Mater. Trans. A* **1996**, *27*, 41–48. [CrossRef]
21. Miracle, D.B. The efficient cluster packing model—An atomic structural model for metallic glasses. *Acta Mater.* **2006**, *54*, 4317–4336. [CrossRef]
22. Zhu, B.; Wang, X.; Li, X.; Wang, D.; Qin, Y.; Han, F. Bulk amorphous $Al_{75}V_{12.5}Fe_{12.5-x}Cu_x$ alloys fabricated by consolidation of mechanically alloyed amorphous powders. *J. Alloys Compd.* **2014**, *586*, 645–649. [CrossRef]
23. Inoue, A. Stabilization of metallic supercooled liquid and bulk amorphous alloys. *Acta Mater.* **2000**, *48*, 279–306. [CrossRef]

24. Takeuchi, A.; Inoue, A. Classification of bulk metallic glasses by atomic size difference, heat of mixing and period of constituent elements and its application to characterization of the main alloying element. *Mater. Trans.* **2005**, *46*, 2817–2829. [CrossRef]
25. Zhang, Y.; Zhou, Y.J.; Lin, J.P.; Chen, G.L.; Liaw, P.K. Solid-Solution Phase Formation Rules for Multi-component Alloys. *Adv. Eng. Mater.* **2008**, *10*, 534–538. [CrossRef]
26. Lu, Z.P.; Liu, C.T. A new glass-forming ability criterion for bulk metallic glasses. *Acta Mater.* **2002**, *50*, 3501–3512. [CrossRef]
27. Zhang, W.; Chen, S.; Zhu, Z.; Wang, H.; Li, Y.; Kato, H.; Zhang, H. Effect of substituting elements on thermal stability and glass-forming ability of an Al-based AlNiEr metallic glass. *J. Alloys Compd.* **2017**, *707*, 97–101. [CrossRef]
28. Kissinger, H.E. Reaction Kinetics in Differential Thermal Analysis. *Anal. Chem.* **1957**, *29*, 1702–1706. [CrossRef]
29. Ozawa, T.A. New method of analyzing thermogravimetric data. *Bull. Chem. Soc. Jpn.* **1965**, *38*, 1881–1886. [CrossRef]